A COMPARATIVE INVESTIGATION BETWEEN THE MCSA METHOD AND THE HILBERT TRANSFORM FOR BROKEN ROTOR BAR FAULT DIAGNOSTICS, IN A CLOSED-LOOP THREE-PHASE INDUCTION MOTOR

Lachtar SALAH[1], Ghoggal ADEL[2], Koussa KHALED[3], Bouraiou AHMED[4]

Although it is one of the most common fault signatures methods for diagnosing motor defects, Motor Current Signals Analysis (MCSA) has some drawbacks that can degrade the performance and accuracy of a motor diagnostics system. In particular, it is very difficult to detect broken rotor bars (BRB) when the motor operates at no load condition. This paper proposes a comparative study of two methods for the diagnosis of BRB defect in closed-loop induction motors. Stator currents in an induction motor have been measured, transferred to a computer, used for MCSA, and advanced signal-processing algorithms. They consist of analyzing the envelope of one-stator phase current. This envelope is obtained, using the Hilbert transformation (HT). Both methods are based on spectral analysis via Fast Fourier Transform (FFT). Both methods have proved their effectiveness to detect BRBs under different load conditions. However, the HT is considered more efficient compared to the MCAS method in the case where the motor operating at no load condition. The simulation results obtained for the two methods applied on a three-phase squirrel-cage induction motor controlled are discussed.

Keywords: SCIM, DTC control, BRB diagnostics, MCSA, HT

1. Introduction

Squirrel cage induction motor (SCIM) is widely used in the energy conversion and industrial drive fields because of their robustness, mass power, and cost. Their maintenance and diagnosis become an economic challenge [1–3]. Hitherto, The induction motor is still prone to some drawbacks due to electrical, mechanical, thermal, magnetic and environmental constraints causing internal and/or external defects during the operating processes [4]. It is important to detect

[1] Ph.D Student., LGEB- laboratory, Dept.of Electrical Engineering, University of Biskra, Algeria, e-mail: lachtarsalahba@gmail.com

[2] Prof As., LGEB- laboratory, Dept.of Electrical Engineering, University of Biskra, Algeria, e-mail: ghoetudes@yahoo.fr

[3] Ph.D Student., Unité de Recherche en Energie Renouvelables en Milieu Saharien, URERMS, Centre de Développement des Energies Renouvelables, CDER, 01000 Adrar, Algeria, e-mail: koussakhaled@gmail

[4] Ph.D., Unité de Recherche en Energie Renouvelables en Milieu Saharien, URERMS, Centre de Développement des Energies Renouvelables, CDER, 01000 Adrar, Algeria, e-mail: bouraiouahmed@gmail.com

early the defects that can appear in these machines and therefore develop preventive diagnostic techniques to prevent total machine failure.

Recently, despite considerable improvements in the design and build quality of stator windings to mitigate common electrical stator faults, the design of squirrel cage rotor has undergone few improvements, reasoning that its failures represent a high percentage of the total IM failures [1,5]. The BRB defect is one of the important defects that require early detection because of its unexpected severe damage. Surveys have been revealed that the percentage of this failure accounts for 10% of induction motor faults [6].

The development of robust fault diagnosis techniques under the impact of the control system is one of the challenges of many researchers [7]. When SCIM drivers are used, the control structure of the system becomes more complex and most of the techniques previously tested in open-loop drives are not effective [4,8], only if the stator current spectrum is used in case of anomalies. In DTC-fed SCIM, the stator current spectrum has a high additional frequency component due to the effects of control parameters and switching frequency, which is responsible for the space vector modulation (SVM) of the inverter [2]. Although their amplitude will be affected by control structures and parameters, sidebands around the supply frequency of the phase current and voltage can still be used for BRB fault detection [9,10].

Many techniques have been developed for the BRB defect using several fault signatures such as motor current, vibration, acoustic noise and magnetic flux [11]. One of the most common fault signatures for detecting BRBs in an induction motor is MCSA for detecting sidebands around the supply frequency[12,13]. When BRB fault occurs, current components are induced in the stator winding at frequencies given by:

$$f_b = (1 \pm 2ks) f_s, \quad k = 1,2,3,\ldots \tag{1}$$

Where f_s is the supply frequency and s is the slip. MCSA is one of the most widely used methods in the last decade to detect sidebands around the power frequency, without estimating motor parameters, online in a motor drive system, it becomes the main for on-line motor diagnostics. However, this technique has some drawbacks such as spectral leakage due to the finite-time window, need for a high-frequency resolution, and variation in the sideband frequencies due to the varying load conditions [1,14]. MCSA using FFT technique cannot detect the component of the characteristic frequencies of BRBs fault, which is very close to the fundamental frequency when the motor operating at no load condition [15].

This paper addressed the HT, which can be considered, as a promising BRB fault diagnostic technique that will be proposed in order to overcome the aforementioned difficulties especially at very low slip [6,16]. It offers very low sensitivity to the low-level load condition compared to MCSA. This technique is based on the analysis of the envelope of a single stator phase current for BRBs

fault [2]. The envelope is obtained from the modulation of the stator phase current. The investigation revealed that this envelope is a powerful feature for BRBs fault.

The main purpose of this paper is to the diagnosis of the broken rotor bars fault when the closed-loop induction motor operates at low slip. It is suitable that this diagnostic technique is non-invasive and requires only an acquisition of these readily available signals in the motor control system. The DTC control strategy is presented to preserve high-performance control over output quantities, especially in torque and speed. The proposed diagnostic approach is based on the comparison of the signature analyses of both MCSA and MCSA via HT used the stator currents. It is a simple diagram, independent of the motor parameter, proposed to effectively detect BRBS faults in the DTC-fed SCIM at any load conditions. Simulation results are presented to confirm the effectiveness and the feasibility of the HT strategy that offers the possibility to detect BRBs fault even at no-load condition compared to CMSA.

2. SCIM model including BRB fault

The broken bar fault in the SCIM is modeled based on the winding function approach WFA. All the space harmonics in the machine are taken into account. The WFA approach predicts the performances of the differential equations model. This model refers to the coupled magnetic approach by treating the current in each rotor bar as an independent variable [17]. The induction motor model is considered with the following simplifying assumptions [18]:

- The magnetic circuits are unsaturated,
- The inter-bar current is neglected,
- the skin effects are neglected,
- The effect of slots is neglected,
- The distribution of the magnetomotive force in the air-gap is sinusoidal.

The rotor squirrel-cage modeling is based on the equivalent diagram of (N_r+1) meshes as shown in Fig. 1. Each mesh is substituted by an equivalent circuit represented by a rotor bar and a segment of end-ring, respectively under resistive and inductive nature (R_b, R_e, L_b, L_e).

R_b *and* L_b, *r*epresent the rotor bar resistance and inductance. R_e *and* L_e are the end-ring segment resistance and its inductance. The rotor voltage equations of the N_r loops can be expressed as follow:

$$\left(2R_{ek} + R_{b(k+1)} + R_{bk}\right)I_{rk} - R_{bk}I_{r(k-1)} - R_{b(k+1)}I_{r(k+1)} - R_eI_{e(N_r+1)} + \frac{d\phi_{rk}}{dt} = 0 \qquad (2)$$

Where ϕ_{rk} is the rotor flux crossing the rotor loop *k*.

The dynamic mathematical model of the induction motor can be written in vector matrix as:

$$[V]=[R][I]+\frac{d}{dt}([L][I]) \tag{3}$$

Where the voltage vector matrix [*V*] is given by:

$$[V]=[[V_s]\quad[V_r]]\leftrightarrow\begin{cases}[V_s]=[v_{sa}\quad v_{sb}\quad v_{sc}]^T\\ [V_r]=[v_{r1}\quad v_{r2}\quad\dots\quad v_{rN_r}\quad v_{re}]^T_{(1xN_r+1)}=0\end{cases} \tag{4}$$

Where N_r is the number of rotor bars.

Fig. 1. The equivalent circuit of the rotor squirrel-cage

The current vector matrix [I] is composed:

$$[I]=[[I_s]\quad[I_r]]\leftrightarrow\begin{cases}[I_s]=[i_{sa}\quad i_{sb}\quad i_{sc}]^T\\ [I_r]=[I_{r1}\quad I_{r2}\quad\dots\quad I_{rN_r}\quad I_e]^T_{(1xN_r+1)}=0\end{cases} \tag{5}$$

The global resistance matrix [*R*] is given as follow:

$$[R]=\begin{bmatrix}[R_s] & [0]_{(3,N_r+1)}\\ [0]_{(3,N_r+1)} & [R_r]\end{bmatrix} \tag{6}$$

Where, [R_s] is the diagonal matrix of the stator resistances phases of (*m*, *m*) dimensions.

$$[R_s]=\begin{bmatrix} R_{s1} & 0 & 0 \\ 0 & R_{s2} & 0 \\ 0 & 0 & R_{s3} \end{bmatrix} \tag{7}$$

R_{s1}, Rs_2, and R_{s3} are the identical resistances of stator phases winding.
The resistance $[R_r]$ is a symmetric matrix (N_r+1, N_r+1) given as:

$$[R_r]=\begin{bmatrix} R_{rr} & -R_b & 0 & 0 & -R_{b(1,N_r)} & -R_{e(1,N_r+1)} \\ -R_b & R_{rr} & -R_b & \vdots & 0 & -R_e \\ 0 & -R_b & R_{rr} & -R_b & \vdots & \vdots \\ \vdots & 0 & -R_b & \ddots & -R_b & \vdots \\ -R_{b(N_r,1)} & \vdots & 0 & -R_b & R_{rr(N_r,N_r)} & \vdots \\ -R_{e(N_r+1,1)} & -R_e & -R_e & -R_e & -R_e & -R_{e(N_r+1,N_r+1)} \end{bmatrix} \tag{8}$$

Where, $R_{rr}=2(R_b+R_e)$, R_b is the rotor bar resistance and R_e is the end ring resistance.
The global inductance matrix $[L]$ is as follow:

$$[L]=\begin{bmatrix} [L_s] & [M_{sr}]_{(3,N_r+1)} \\ [M_{rs}]_{(N_r+1,3)} & [L_r]_{(N_r+1,N_r+1)} \end{bmatrix} \tag{9}$$

Where the inductance matrix $[L_s]$is given by:

$$[L_s]=\begin{bmatrix} L_{s1} & M_s & M_s \\ M_s & L_{s2} & M_s \\ M_s & M_s & L_{s3} \end{bmatrix} \tag{10}$$

Where, L_{s1}, $L_{s2,}$ and L_{s3} are the identical proper inductances of the stator coil and M_s is the mutual inductance of the stator phases. The inductance matrix $[L_r]$ is a symmetric matrix (N_r+1, N_r+1) given by:

$$[L_r]=\begin{bmatrix} L_{rr} & M_T & M_{rr} & \cdots & M_T & -L_{e(1,N_r+1)} \\ M_T & L_{rr} & M_T & M_{rr} & M_{rr} & -L_e \\ M_{rr} & M_T & L_{rr} & M_T & \vdots & \vdots \\ \vdots & M_{rr} & M_T & \ddots & M_T & \vdots \\ M_T & \vdots & M_{rr} & M_T & L_{rr(N_r,N_r)} & \vdots \\ -L_{e(N_r+1,1)} & -L_e & -L_e & -L_e & -L_e & -L_{e(N_r+1,N_r+1)} \end{bmatrix} \tag{11}$$

Where, $L_{rr}= L_{mr}+2(L_b+L_e)$, $M_T =(M_{rr}- L_b)$, L_{mr} is the magnetizing inductance of each rotor loop. L_b is the rotor bar leakage inductance, L_e is the rotor end ring leakage inductance and M_{rr} is the mutual inductance between two rotor loops.
The mutual inductance matrix [M_{sr}], between the stator windings and rotor loops of (3, N_r+1) dimensions, which signified that the vector of the rotor currents comprises (k+1) elements corresponding to the number of rotor cage bars N_r, plus the end-ring loop (N_r+1).

$$\left[M_{sr}\right]=\begin{bmatrix} M_{s1rk} & M_{s1rk+1} & \cdots M_{s1rN_r+1} \\ M_{s2rk} & M_{s2rk+1} & \cdots M_{s2rN_r+1} \\ M_{s3rk} & M_{s3rk+1} & \cdots M_{s3rN_r+1} \end{bmatrix} \tag{12}$$

The mechanical rotor equations of velocity Ω_r and position Θ_r are represented as follows:

$$\begin{cases} J\dfrac{d\Omega_r}{dt} = T_e - f_v\Omega_r - T_L \\ \dfrac{d\theta_r}{dt} = \Omega_r \end{cases} \tag{13}$$

Where J is the moment of inertia, T_L is the load torque and T_e the electromagnetic torque produced by the machine is obtained by:

$$T_e = 0.5\left[I\right]^T \frac{d\left[L(\theta_r)\right]}{d\theta_r}\left[I\right] \tag{14}$$

The mathematical model of induction motor is presented as follow:

$$\begin{bmatrix}[V] \\ -T_r \\ 0\end{bmatrix}=\begin{bmatrix}[R(\theta_r)] & [0] & [0] \\ -0.5[I]^T\dfrac{d[L(\theta_r)]}{d\theta_r} & f_v & 0 \\ [0] & -1 & 0\end{bmatrix}\begin{bmatrix}[I] \\ \Omega_r \\ \theta_r\end{bmatrix}+\begin{bmatrix}[L(\theta_r)] & [0] & [0] \\ [0] & J & 0 \\ [0] & 0 & 1\end{bmatrix}\frac{d}{dt}\begin{bmatrix}[I] \\ \Omega_r \\ \theta_r\end{bmatrix} \tag{15}$$

In order to simulate the broken rotor bars failure using MATLAB software, the broken bar resistance R_b is strongly increased by an additional resistance R_{bF} called the defect resistance.

3. DTC strategy fed induction motor

Mainly the DTC method illustrated in Fig. 2 has selected one of the six non-zeroes and two zero voltage vectors of the inverter based on the instantaneous errors in torque and stator flux magnitude Fig. 3. This is done by choosing the appropriate sector in the spatial vector modulation that will be described in this section.

The DTC strategy is based on the estimation of the magnetic flux and the torque from the measurement of the voltages and currents supplying the motor. If the torque or flux falls out of a predefined tolerance range (hysteresis band), the variable speed drive transistors are switched to the next state in such a way as to return to the range as quickly as possible [19,20].

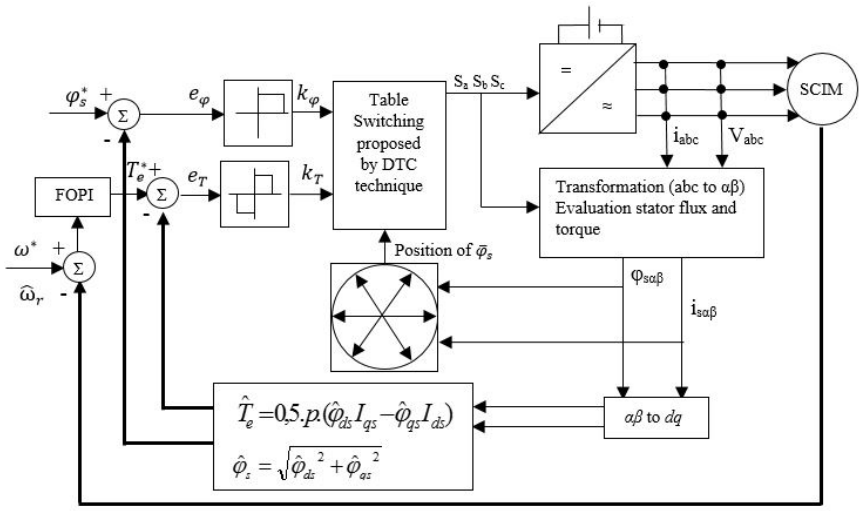

Fig. 2. DTC block diagram fed SCIM

In a three-phase inverter of two levels voltage, the voltage measured between the output of each branch and the neutral point can have two values, V_{dc} or V_{k0} with:

$$V_{k0} = S_k V_{dc} \tag{16}$$

Where S_k the signal controls k connects, and V_{dc} the voltage rectified at the entry of the inverter.

The operation can be described as follow:

S_k =1: Switch top is closed, and switch bottom is open.

S_k =0: Switch top is opened, and switch bottom is closed.

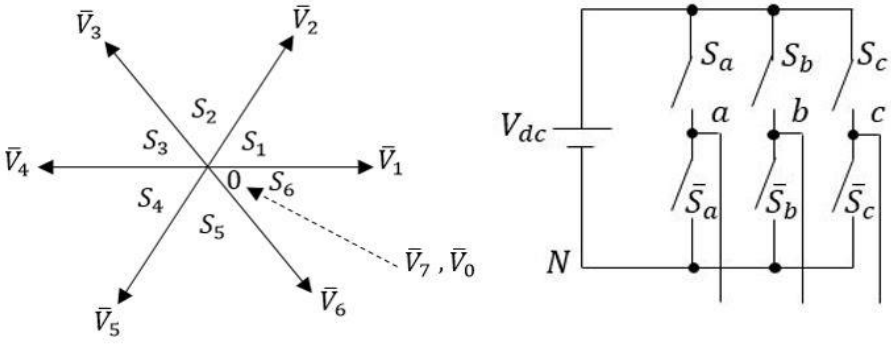

Fig. 3. Inverter output voltage sectors

Admitting that the point (*N*) is neutral, the voltage of the neutral line can be evaluated as follow:

$$\begin{bmatrix} V_{1n} \\ V_{2n} \\ V_{3n} \end{bmatrix} = \frac{1}{3} V_{dc} \begin{bmatrix} 2S_a & -S_b & -S_c \\ -S_a & 2S_b & -S_c \\ -S_a & -S_b & 2S_c \end{bmatrix} \tag{17}$$

The application of the Clarke frame allows the establishment of (1, 2, 3→ α, β).

$$\begin{bmatrix} V_\alpha \\ V_\beta \end{bmatrix} = V_{dc} \begin{bmatrix} S_a & -\frac{1}{2}S_b & -\frac{1}{2}S_c \\ 0 & \sqrt{\frac{1}{2}}S_b & -\sqrt{\frac{1}{2}}S_c \end{bmatrix} \tag{18}$$

Therefore, the space voltage vector $\bar{v}_s$ might be written as follow:

$$\bar{v}_s = V_\alpha + jV_\beta = \sqrt{\frac{2}{3}} V_{dc} \left(S_a + S_b e^{j\frac{2}{3}\pi} + S_c e^{-j\frac{2}{3}\pi} \right) \tag{19}$$

3.1 Stator flux controller

The stator flux formula can be written as follow:

$$\bar{\phi}_s = \int_0^t \left(\bar{v}_s - \bar{R}_s \bar{i}_s \right) dt \tag{20}$$

Where:

$$\bar{i}_s = I_{s\alpha} + jI_{s\beta} = \sqrt{\frac{2}{3}} I_{dc} \left(S_a + S_b e^{j\frac{2}{3}\pi} + S_c e^{-j\frac{2}{3}\pi} \right) \tag{21}$$

Noting that I_{dc} is the current supply the inverter, between two switches of the inverter switches, the selected voltage vector is always the same, hence:

$$\bar{\phi}_s = \bar{\phi}_{s0} + \int_0^t \left(\bar{v}_s - \bar{R}_s \bar{i}_s \right) dt \tag{22}$$

Where $\bar{\phi}_s$ is the flux vector, $\bar{\phi}_{s0}$ is the initial vector of $\bar{\phi}_s$ and, $\bar{R}_s$ is the stator resistance.

If the voltage drop due to the stator resistance neglected, $\bar{\phi}_s$ can be written as follow:

$$\bar{\phi}_s = \bar{\phi}_{s0} + \int_0^t \bar{v}_s \, dt \tag{23}$$

Noting that over an interval ($t=0$ to $t=t_e$), the end of the $\bar{\phi}_s$ vector moves on a line whose direction is given by the selected vector $\bar{v}_s$ during t_e Fig. 4.

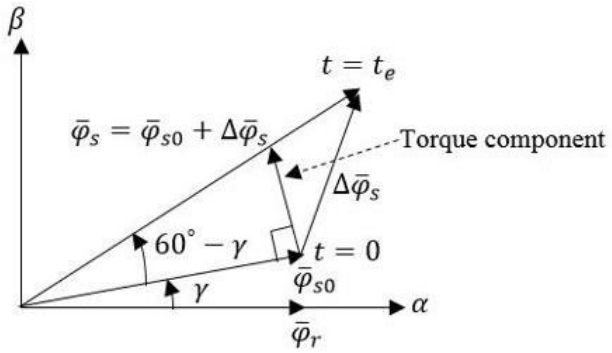

Fig. 4. Space vectors of stator and rotor fluxes

The estimated flux is carried out by the integration of the stator voltage. The selection of the voltage vector depends on the position of stator flux.

$$\frac{d}{dt}\begin{bmatrix}\hat{\phi}_{s\alpha}\\ \hat{\phi}_{s\beta}\end{bmatrix}=\begin{bmatrix}V_{s\alpha} & -R_s I_{s\alpha}\\ V_{s\beta} & -R_s I_{s\beta}\end{bmatrix} \tag{24}$$

$$\hat{\phi}_s=\sqrt{\hat{\phi}_{s\alpha}^2+\hat{\phi}_{s\beta}^2} \tag{25}$$

3.2 Torque Controller

The electromagnetic torque component as shown in Fig. 4, is a sinusoidal function of γ, the angle between the stator and rotor fluxes $\bar{\phi}_s$ and $\bar{\phi}_r$. Since the stator flux variation is faster than that of the rotor flux, which will produce a variation of the developed torque due to the variation of the angle γ between the two vectors. The electromagnetic torque equation is given by:

$$T_e=\frac{1}{2}P\bar{i}_s j\bar{\phi}_s \tag{26}$$

Since S_i the area in which the vector is located is determined by the $\hat{\phi}_{s\alpha}$ and $\hat{\phi}_{s\beta}$ equation components (25). The electromagnetic torque can be estimated by means of equation (27):

$$\hat{T}_e=P(\hat{\phi}_{s\alpha}I_{s\beta}-\hat{\phi}_{s\beta}I_{s\alpha}) \tag{27}$$

The output of the hysteresis bands must indicate the direction of the $\bar{\phi}_s$ module evolution and torque $\hat{T}_e$, in order to select the corresponding voltage vector (Fig. 3).

3.3 Sequences of the switching table

Based on the hysteresis state of the torque and the flux and the switching sector of the stator flux, which is designated by (α), the DTC algorithm (Fig. 2) selects the suitable inverter voltage vector to apply to the induction motor from the Table 1. The outputs of the switching vectors in the different stator flux sectors are parameters for the inverter switching devices.

$$\alpha = \angle \bar{\phi}_s = \tan^{-1}\left(\frac{\phi_{s\beta}}{\phi_{s\alpha}}\right) \tag{28}$$

The active switching vectors are $\bar{V}_1 \to \bar{V}_6$, and the zero switching vectors are $\bar{V}_0$, $\bar{V}_7$ as shown in table 1.

Table 1

Switching sequences of inverter voltage vectors

Sector (S)		1	2	3	4	5	6
$k_{\varphi=1}$	$k_{T=1}$	110	010	011	001	101	100
	$k_{T=0}$	111	000	111	000	111	000
	$k_{T=-1}$	101	100	110	010	011	001
$k_{\varphi=0}$	$k_{T=1}$	010	011	001	101	100	110
	$k_{T=0}$	000	111	000	111	000	111
	$k_{T=-1}$	001	101	100	110	010	011

Considering the six sectors shown in Table 1, the stator flux switching sectors can be distributed as follow:

$$\alpha = \begin{cases} -30^0 < \alpha_1 < 30^0 \\ 30^0 < \alpha_2 < 90^0 \\ 90^0 < \alpha_3 < 150^0 \\ 150^0 < \alpha_4 < 210^0 \\ 210^0 < \alpha_5 < 270^0 \\ 270^0 < \alpha_1 < 330^0 \end{cases}$$

4. Simulation results for both healthy and faulty cases

The simulation of the closed loop SCIM in MATLAB/Simulink software in order to calculate easily the stator three-phase currents, torque and rotor speed in both cases healthy and faulty appearing respectively in Figs. 5 and Figs. 6. The diagnosis process of the BRB fault is verified under two different techniques. For the DTC fed SCIM system, the constant control is adopted which has the ability to adjust the motor reference speed. The fundamental frequency is corresponding to rotor speed level.

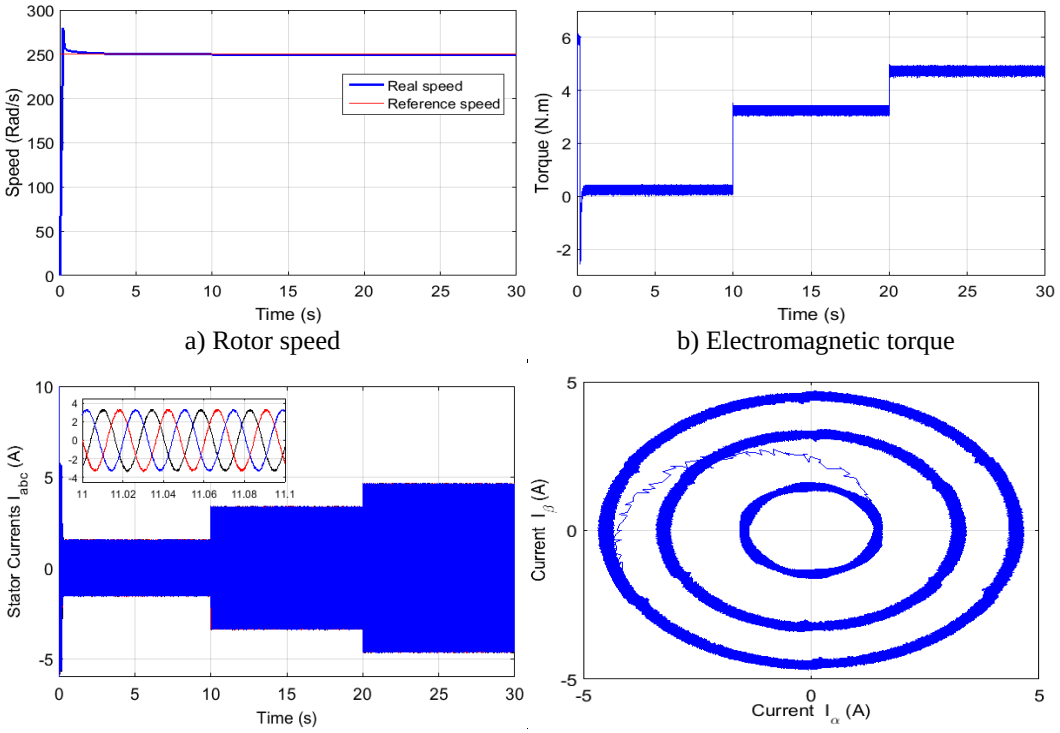

a) Rotor speed b) Electromagnetic torque

c) Stator phases currents d) Quadratic currents component (α,β)

Figs. 5. Electrical and mechanical quantities of the SCIM under DTC strategy in the healthy case

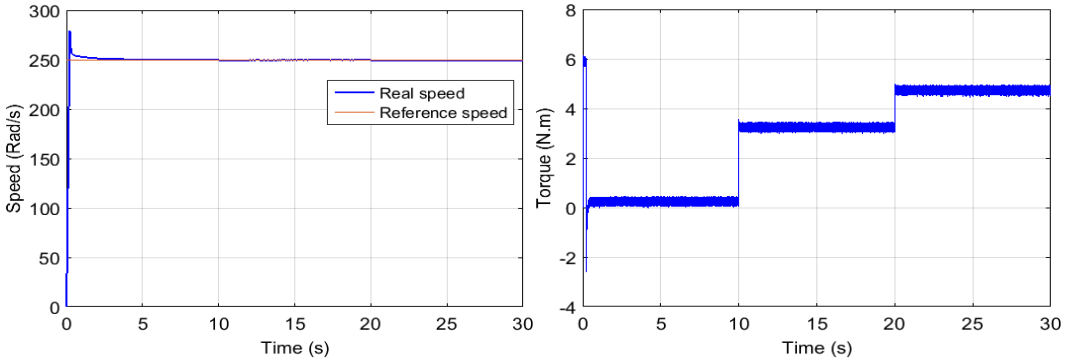

a) Rotor speed b) Electromagnetic torque

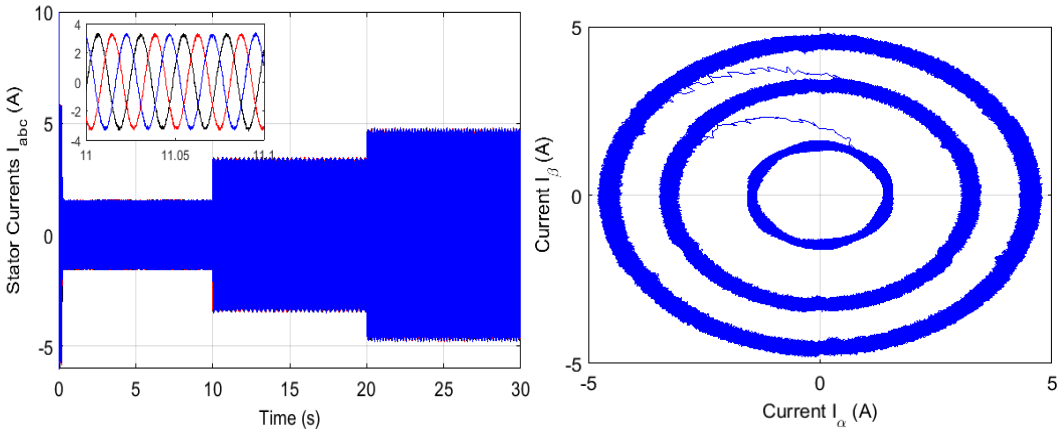

c) Stator phases currents d) Quadratic current component (α,β)

Figs. 6. Electrical and mechanical quantities of the SCIM under DTC strategy in faulty case

4.1 Hilbert transform for detection BRBs fault

The HT method is used in various scientific areas such as signal transmission, geophysical data processing, fault detection and diagnosis in induction motors and others [1]. One of these scientific areas is the diagnosis of BRBs fault in the rotor cage in induction motors [15,16]. Discussion and application of the HT for the stator current analysis of SCIM under closed-loop are introduced as follows.

$$Ht(i_{sa}(t)) = \frac{1}{\pi}\int_{-\infty}^{+\infty}\frac{i_{sa}(\tau)}{t-\tau}d\tau \tag{29}$$

Where $Ht(i_{sa}(t)) = \hat{i}_{sa}(t)$ is the $i_{sa}(t)$ imaginary signal, the divergence $t=\tau$ is enabled by taking the Cauchy principal value of the integral.

By coupling the $i_{sa}(t)$ real signal with its imaginary $\hat{i}_{sa}(t)$, the analytical signal $\bar{i}_{sa}(t)$ is created:

$$\bar{i}_{sa}(t) = i_{sa}(t) + j\hat{i}_{sa}(t) = a(t)e^{j\theta(t)} \tag{30}$$

Where:

$$a(t) = \sqrt{i_{sa}^2(t) + \hat{i}_{sa}^2(t)} \quad \text{and} \quad \theta(t) = \tan^{-1}\left(\frac{i_{sa}(t)}{\hat{i}_{sa}(t)}\right) \tag{31}$$

Where $a(t)$ is the so-called envelope ($\bar{i}_{sa}(t)$ instantaneous amplitude), that can reflect the $i_{sa}(t)$ energy varies with time and $\theta(t)$ is the instantaneous phase of $\bar{i}_{sa}(t)$.

The procedure to obtain the one phase stator current envelope for BRB case for diagnostic and analyzing can be summarised in the following steps:
The first step, computation the HT of the phase stator current $i_{sa}(t)$, in order to get the imaginary signal $\hat{i}_{sa}(t)$ as explaining the aforementioned. The phase stator current is measured for a DTC fed IM in the healthy and faulty cases under different load conditions as shown in Fig. 5 (c) and Fig. 6 (c). The second step, modulation of the complex phase stator current (29) is necessary to obtain the so-called envelope $a(t)$ such as seen in Figs. 7. The identification of the envelope consists of extracting only the positive peak of each period of the phase stator current. The third step, a Low-Pass Filter is needed to eliminate a high-frequency component due to the frequency of the space vector modulation (SVM) of the DTC inverter. As a general rule, the fundamental frequency of the stator current varies from 0 to 50 Hz and the sampling frequency in our case went up to 4 kHz, caused by the hysteresis bands of flux and torque. This SVM component is removed from the envelope signal by a second-order low-pass filter. As a result, the envelope is isolated from the phase stator current without a significant SVM component. The last step, the normalization of the envelope signal by removing the dc component.

$$i_{env}(t) = a(t)^* - mean\left(a(t)^*\right) \tag{32}$$

Where: $a(t)^*$ is the filtered signal $a(t)$

Therefore, the identified envelope is useful as an indicator to detect BRBs fault. A fast Fourier transform (FFT) is applied to the identified envelope to detect BRBs fault at a specific frequency band, which is low to the supply frequency.

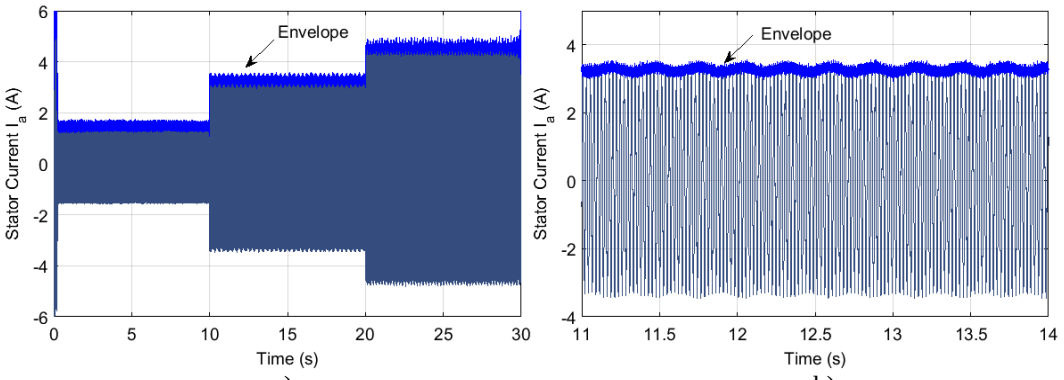

Figs. 7. a) Stator current Ia and its envelope for one BRB under different load condition, and b) Its zoom

Using the HT of the stator current or its modulus and apply it for detection the asymmetries rotor fault, particularly, at no-load condition has significant

advantages compared with the MCSA method [6,16]. Otherwise, this paper focuses on the diagnosis of the rotor asymmetries at low load in SCIM drive and the resolution of the difficulties related when the SCIM operating under high frequencies caused by the switching closed-loop strategy [2,8,22].
The simulation was done under the software Matlab / Simulink for a healthy case and a one BRB faulty case are shown respectively in Figs. 5 and Figs. 6. In both cases, the tests were carried out under the no load, 50% load and 75% load conditions, to demonstrate the feasibility of the proposed method in the no-load state.
The simulated three-phase SCIM was a, 3.6 kW, 50 Hz, 380 V, two-poles and with 48 stator slots 28 rotor bars.

Table 2

Simulation tests of the healthy and faulty motor under DTC strategy

Motor	Load	Slip %	$2sf_s$ (Hz)	$(1\pm2s)f_s$ (Hz)
Healthy case	No load	-	-	-
Faulty case One BRB	No load	0.34	0.34	-
	50% load	3.62	3.62	37.96 45.13
	75% load	5.37	5.37	37.04 47.72

The rotation speed of the SCIM operating under DTC strategy is fixed at 250 rad/s Fig. 5 (a), in the healthy case under the no-load condition the fundamental frequency corresponding to the speed rotation is 40 Hz seen in Fig. 8 (a).

The results are presented in the form of normalized spectra in Figs. 8 and Figs. 9 are obtained by the Fast Fourier Transform (FFT) algorithm in a linear scale with the Hamming Window. In fact, Figs. 8 present the FFT of the classical method phase current (MCSA), and Figs. 9 present the FFT of the phase current envelope filtered $i_{env}(t)$ (proposed method).

Figs. 8 present the results of the stator phase current processing. The components of the frequency characteristic of the BRB condition are completely buried at the no-load condition under the mains frequency component spectral leakage, which clearly appearing similarity in both Fig. 8 (a) and Fig. 8 (b) respectively healthy case and BRB case. The increasing of the load is corresponding to the increase in the motor slip (show Table 2), which makes the frequency characteristic components of the BRB clearly shown in Fig. 8 (c) and Fig. 8 (d) respectively under 50% and 75% load conditions. Concluding, according to both results whether in table 2 or in Figs. 8, the classical MCSA method is unable to detect the BRB fault at the no-load or even at the low-load condition. On the other hand, this method is efficient to detect asymmetries rotor at a high level-load.

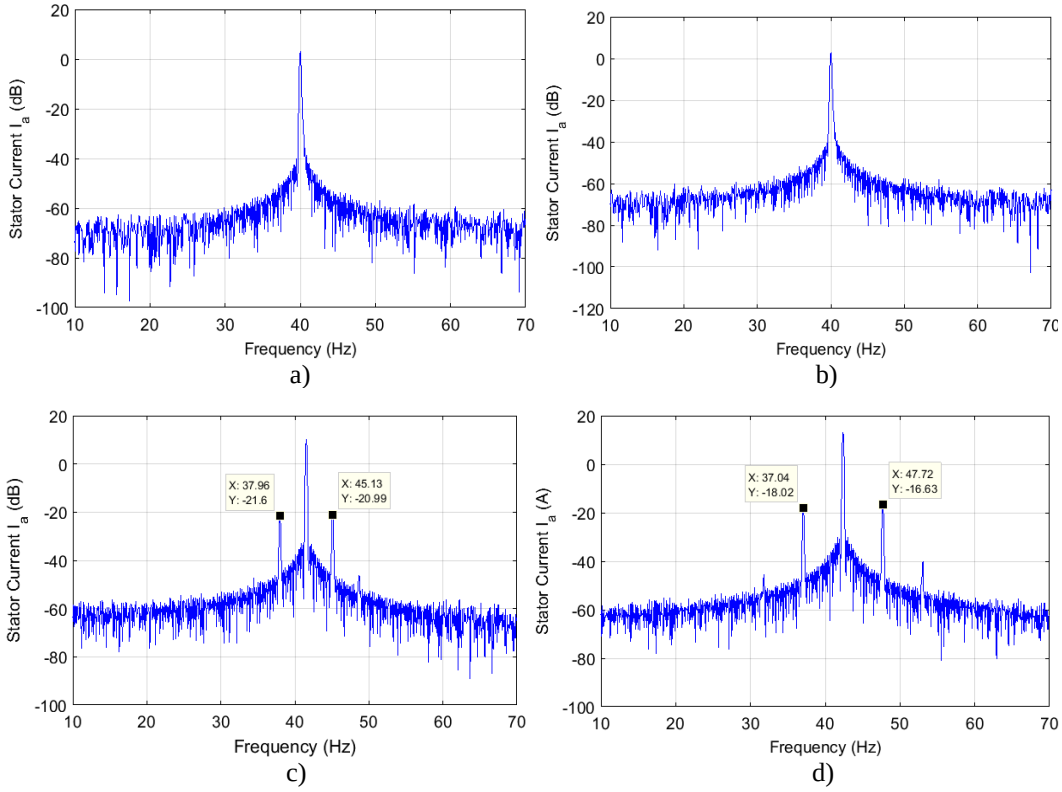

Figs. 8. The spectrum of the phase current under a DTC strategy: a) and b) respectively healthy motor and one BRB at no-load condition, c) one BRB at 50% load condition, d) one BRB at 75% load condition

The proposed method relies on the analysis of the stator phase current oscillations illustrated by its positive peaks (envelope). Figs. 9 present the results of the identified envelope processing. in healthy case, Fig. 9 (a) presents that there is not any specific frequency associated with BRB fault. The frequency characteristic components related to BRB fault is clearly shown in Fig. 9 (b) compared to Fig. 8 (b) at no load condition. In conclusion, the proposed method is able to detect the frequency characteristic related to the BRB fault at any load condition, even at the absolute no-load condition.

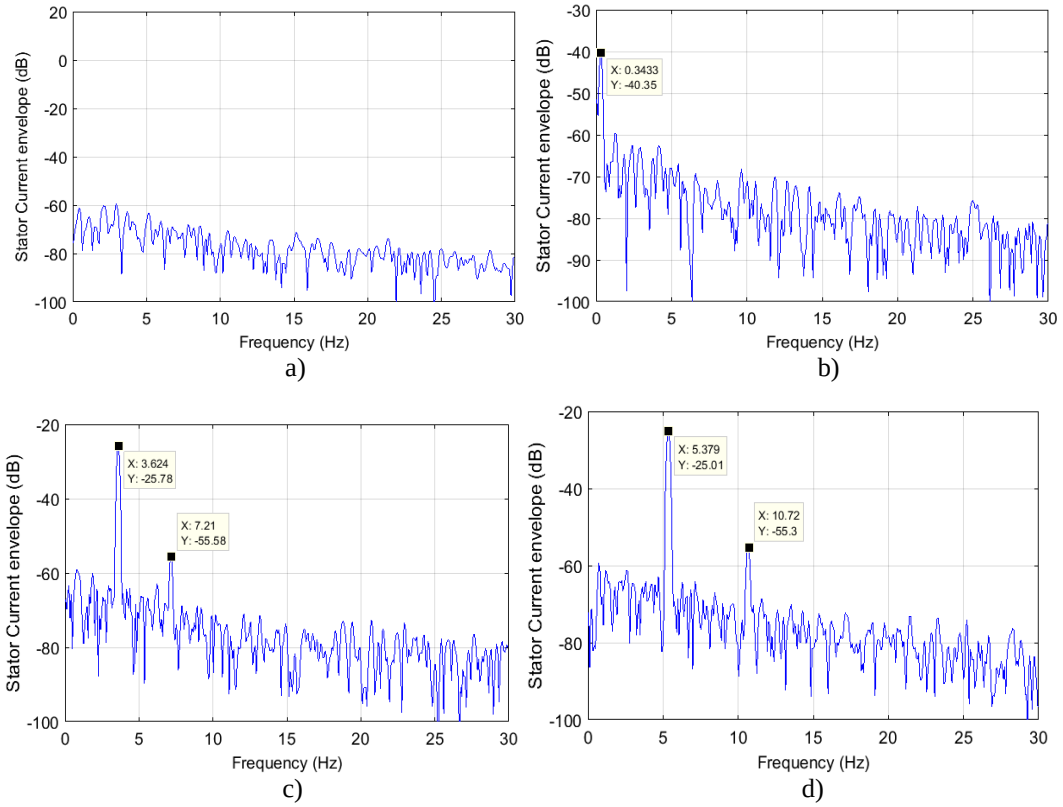

Figs. 9. The spectrum of the phase current filtered envelope under a DTC strategy: a) and b) respectively healthy motor and one BRB at no-load condition, c) one BRB at 50% load condition, d) one BRB at 75% load condition

5. Conclusion

This paper has presented a motor fault diagnosis method based on stator phase current and its envelope for BRBs for SCIM controlled by DTC strategy. Rotor fault signatures were generated using the classical method MCSA and HT method. The classical method proved its failure to detect the BRB fault at the no-load condition. The spectrum leakage of the fundamental frequency hides the fault frequency characteristic components. However, analysis at no-load of the SCIMs under closed-loop industrial applications is very interesting, required unconventional techniques able to detect motor faults. Therefore, the identified envelope of the stator phase current, based on the HT, have been used to perform MCSA, as an unconventional technique in this paper. This method proved its effectiveness to detect BRB frequency characteristic components at any load condition, even at the absolute no-load condition, as it requires only a single stator phase current and a limited storage memory. These advantages make it appropriate for software and hardware implementations.

REFERENCES

[1].*R. Puche-Panadero, M. Pineda-Sanchez, M. Riera-Guasp, J. Roger-Folch, E. Hurtado-Perez and J. Perez-Cruz*,"Improved resolution of the MCSA method via Hilbert transform, enabling the diagnosis of rotor asymmetries at very low slip",IEEE Trans Energy Convers 2009;24:52–9. doi:10.1109/TEC.2008.2003207.

[2].*A M. da Silva, R. J Povinelli and N A. O Demerdash*,"Induction machine broken bar and stator short-circuit fault diagnostics based on three-phase stator current envelopes",IEEE Trans Ind Electron 2008;55:1310–8. doi:10.1109/TIE.2007.909060.

[3].*H A. Toliyat, M S. Arefeen and A G. Parlos*,"A method for dynamic simulation of air-gap eccentricity in induction machines",IEEE Trans Ind Appl 1996;32:910–8. doi:10.1109/28.511649.

[4].*H. Talhaoui, A. Menacer, A. Kessal and R. Kechida*,"Fast Fourier and discrete wavelet transforms applied to sensorless vector control induction motor for rotor bar faults diagnosis",ISA Trans 2014;53:1639–49. doi:10.1016/j.isatra.2014.06.003.

[5].*A. Bellini, F. Filippetti, C. Tassoni and G A. Capolino*,"Advances in diagnostic techniques for induction machines",IEEE Trans Ind Electron 2008;55:4109–26. doi:10.1109/TIE.2008.2007527.

[6].*M. Abd-el-Malek, A K. Abdelsalam and O E. Hassan*,"Induction motor broken rotor bar fault location detection through envelope analysis of start-up current using Hilbert transform",Mech Syst Signal Process 2017;93:332–50. doi:10.1016/j.ymssp.2017.02.014.

[7].*Y. Gritli, A O Di. Tommaso, R. Miceli, F. Filippetti and C. Rossi*,"Closed-loop bandwidth impact on MVSA for rotor broken bar diagnosis in IRFOC double squirrel cage induction motor drives",4th Int Conf Clean Electr Power Renew Energy Resour Impact, ICCEP 2013 2013:529–34. doi:10.1109/ICCEP.2013.6586904.

[8].*M. Drif and A J M. Cardoso*,"Stator fault diagnostics in squirrel cage three-phase induction motor drives using the instantaneous active and reactive power signature analyses",IEEE Trans Ind Informatics 2014;10:1348–60. doi:10.1109/TII.2014.2307013.

[9].*A. Bellini, C. Concari, G. Franceschini and C. Tassoni*,"Different procedures for the diagnosis of rotor fault in closed loop induction motors drives",Proc IEEE Int Electr Mach Drives Conf IEMDC 2007 2007;2:1427–33. doi:10.1109/IEMDC.2007.383638.

[10].*C C M. Cunha and B J C. Filho*,"Detection of Rotor Faults in Squirrel-Cage Induction Motors using Adjustable Speed Drives",Conf Rec 2006 IEEE Ind Appl Conf Forty-First IAS Annu Meet 2006;5. doi:10.1109/IAS.2006.256870.

[11].*S. Nandi, H A. Toliyat and X. Li*,"Condition monitoring and fault diagnosis of electrical motors-A review",IEEE Trans Energy Convers 2005;20:719–29. doi:10.1109/TEC.2005.847955.

[12].*J de J R. Magdaleno, H. Pegrina-Barreto, J M. Ramirez-Cortes, P. Gomez-Gil and R. Morales-Caporal*,"FPGA-based broken bars detection on induction motors under different load using motor current signature analysis and mathematical morphology",IEEE Trans Instrum Meas 2014;63:1032–40. doi:10.1109/TIM.2013.2286931.

[13].*N. Hamad, K F. Brethee, F. Gu and A. D Ball*,"An investigation of electrical motor parameters in a sensorless variable speed drive for machine fault diagnosis",2016 22nd Int Conf Autom Comput ICAC 2016 Tackling New Challenges Autom Comput 2016:329–35. doi:10.1109/IConAC.2016.7604941.

[14].*G. Didier, E. Ternisien, O. Caspary and H. Razik*,"A new approach to detect broken rotor bars in induction machines by current spectrum analysis",Mech Syst Signal Process 2007;21:1127–42. doi:10.1016/j.ymssp.2006.03.002.

[15].*B. Bessam, A. Menacer, M. Boumehraz and H. Cherif*,"Detection of broken rotor bar faults in

induction motor at low load using neural network",ISA Trans 2015;64:241–6. doi:10.1016/j.isatra.2016.06.004.

[16].*B. Xu, L. Sun, L. Xu and G. Xu*,"Improvement of the Hilbert method via esprit for detecting rotor fault in induction motors at low slip",IEEE Trans Energy Convers 2013;28:225–33. doi:10.1109/TEC.2012.2236557.

[17].*P. Shi, Z. Chen, Y. Vagapov and Z. Zouaoui*,"A new diagnosis of broken rotor bar fault extent in three phase squirrel cage induction motor",Mech Syst Signal Process 2014;42:388–403. doi:10.1016/j.ymssp.2013.09.002.

[18].*C. Kral, F. Pirker, G. Pascoli and H. Kapeller*,"Robust rotor fault detection by means of the Vienna Monitoring Method and a parameter tracking technique",IEEE Trans Ind Electron 2008;55:4229–37. doi:10.1109/TIE.2008.2005176.

[19].*A. Ammar, A. Bourek and A. Benakcha*,"Nonlinear SVM-DTC for induction motor drive using input-output feedback linearization and high order sliding mode control",ISA Trans 2017;67:428–42. doi:10.1016/j.isatra.2017.01.010.

[20].*A. Ammar, A. Benakcha and A. Bourek*,"Closed loop torque SVM-DTC based on robust super twisting speed controller for induction motor drive with efficiency optimization",Int J Hydrogen Energy 2017;42:17940–52. doi:10.1016/j.ijhydene.2017.04.034.

[21].*T. Ameid, A. Menacer, H. Talhaoui and Y. Azzoug*,"Discrete wavelet transform and energy eigen value for rotor bars fault detection in variable speed field-oriented control of induction motor drive", ISA Trans 2018:0–1. doi:10.1016/j.isatra.2018.04.019.